Research Article | Vol. 32, No. 13 / 17 Jun 2024 / Optics Express 23416
Optics EXPRESS

Reducing wavelength jitter in white-light seeded femtosecond optical parametric chirped-pulse amplifiers

THOMAS HÜLSENBUSCH,[1,2,*] LUTZ WINKELMANN,[1] TIMO EICHNER,[1] TINO LANG,[1] GUIDO PALMER,[1] AND ANDREAS R. MAIER[1]

[1]*Deutsches Elektronen-Synchrotron DESY, Notkestraße 85, 22607 Hamburg, Germany*
[2]*Department of Physics, University of Hamburg, Luruper Chaussee 149, 22761 Hamburg, Germany*
[*]*thomas.huelsenbusch@desy.de*

Abstract: White light generation (WLG) in bulk material can be used as a versatile broadband seed source for optical parametric chirped pulse amplification (OPCPA) stages. In this case, it is beneficial to optimize the performance of the WLG seeder in combination with the subsequent OPCPA stage. Here, we characterize how small variations in the drive pulse energy affect the white light seeder performance, in particular the wavelength stability of the amplified OPCPA spectrum. To isolate the influence of drive pulse energy on the OPCPA central wavelength, we introduce a phase-sensitive amplitude measurement and carefully optimize the drive pulse focus position (at the bulk) to minimize the sensitivity to the jitter of the drive pulse energy. With additional active stabilization of the delay between pump and seed pulses in the OPCPA, we achieve a central wavelength jitter of 2×10^{-4}. With this performance, our source is an ideal front-end for applications in laser-plasma acceleration or free-electron laser seeding.

1. Introduction

A variety of applications, such as laser-plasma acceleration (LPA) [1,2] and seeding free-electron lasers (FEL) [3], require broadband pulses with excellent central wavelength stability, as fluctuations in the central wavelength of the driving pulses generally degrade the output of the experiment. In LPA, a change in the properties of the driving laser pulse can affect the acceleration conditions, leading to fluctuations in both the electron energy and the electron energy spread [4]. In FEL seeding, central wavelength jitter can cause a mismatch between electron parameters and undulator acceptance criteria, resulting in fluctuations in x-ray intensity [5].

Both LPA and FEL seeding benefit from short pulses (<50 fs) with a relative central wavelength jitter on the order of 10^{-4} [6]. In addition, LPA requires driving laser pulses with good temporal contrast, while wavelength tunability is necessary for FEL seeding [5].

Lasers based on titanium-doped sapphire (Ti:Sa) gain material can routinely provide pulses with durations below 50 fs. However, when amplifying nJ-range pulses from Ti:Sa oscillators in regenerative amplifiers, the temporal contrast is degraded, and gain narrowing limits the spectral bandwidth. To enhance the temporal contrast, cross-polarized wave generation [7] or saturable absorbers [8] may be utilized, although their efficiency is limited.

Optical parametric chirped-pulse amplifiers (OPCPA) have a gain bandwidth that is limited only by the properties of the nonlinear crystal, such as phase matching and transparency [9]. The transfer of energy from the pump to the signal pulse only occurs during the nonlinear process [10], allowing for good temporal contrast to be achieved as no energy is stored in the crystal. However, a broad-band seed source is required to fully exploit the benefits offered by OPCPA

#527895 https://doi.org/10.1364/OE.527895
Journal © 2024 Received 17 Apr 2024; revised 31 May 2024; accepted 3 Jun 2024; published 11 Jun 2024

Optics EXPRESS

technology. These can be Ti:Sa oscillators which also seed neodymium [11] or ytterbium-based amplifiers [12] to create an optically synchronized pump. However, complex synchronization schemes are often required to achieve the same arrival time of pump and seed pulses at the OPCPA stage [12,13].

Another method for generating broadband seed pulses is through white light generation in bulk media [14–16]. The WLG is driven by pulses ranging from tens of femtoseconds [17–19] to single picoseconds [20,21], that self-compress in a bulk medium in space and time until filamentation occurs [16]. The output is spectrally broadened to several hundred nanometers, supporting even shorter pulse lengths at different spectral regions. Filamentation in bulk media can be achieved with pulse energies below 1 µJ for sub-ps pulses at 1 µm wavelength. Only a fraction of the pulse energy delivered by modern ultrafast lasers [22] is required to drive the WLG. The remaining energy can be used as the pump for OPCPA stages. Additionally, the seed pulse energy obtained from WLG driven by ytterbium-based lasers, with a central wavelength of around 800 nm, can be equal to or higher than that of typical Ti:Sa oscillators [23].

OPCPAs driven by industrial grade Yb pump sources are ideal seed lasers for LPA drive lasers due to their spectral flexibility and good temporal contrast. The high gain in short crystals allows for systems with a small footprint and a rugged design. Additionally, generating pump and seed pulses for the OPCPA from the same drive pulse passively stabilizes the timing between these pulses, easing the requirements on synchronization [18,19]. However, the non-linear process in the OPCPA makes the output pulse energy and spectrum sensitive to beam pointing, temporal jitter and other influences. Although some of these issues can be addressed with mechanical design, others are intrinsic to the WLG.

As WLG is a highly nonlinear process, the shape of the broadened spectrum is influenced by driver energy [24], focusing conditions [25] and material parameters [17]. In the normal dispersion regime, group velocity mismatch in the bulk material can influence the arrival time of the seed pulses at the OPCPA stage [12]. It is difficult to identify the individual contribution of each effect to the central wavelength change in the amplified spectrum.

In this paper, we present a characterization of the output properties of WLG, specifically focusing on the variations of drive energy. Shortcomings were found in the optimization of a WLG source without its subsequent OP(CP)A stage, when it is used as a broadband seed source. A phase-sensitive amplitude measurement [26] is introduced to isolate the influence of drive pulse energy on the amplified spectrum after the OPCPA. Using this technique, the focusing lens position of the WLG stage is optimized to minimize the sensitivity of the OPCPA's central wavelength with respect to the drive pulse energy. We present a wavelength-resolved characterization of the energy of the drive pulses on the amplified spectrum at the optimized operation point of the WLG. Additionally, we actively stabilize the delay between the pump and seed pulses in the OPCPA stage. With improved passive stability and active stabilization, we achieve wavelength jitter below the requirements for LPA and FEL seeding of 2×10^{-4}.

2. Experimental setup

2.1. White light generation

The laser setup used for the measurements is depicted in Fig. 1. It is identical to the first stage of the laser system presented in [27]. The OPCPA system is driven by a ytterbium laser system (Light Conversion PHAROS) delivering femtosecond pulses with 1 mJ of pulse energy. The laser consists of a Kerr-lens modelocked oscillator and a regenerative amplifier (RA). The RA and the pulse picker Pockels cell (PP) are operated on sub-harmonic frequencies of the laser oscillators repetition rate. The pulses are positively chirped to a duration of approximately 500 fs full width at half maximum (FWHM). The transmission through the PP Pockels cell after the RA depends on the applied high voltage, which can be set/modulated from an external input.

Optics EXPRESS

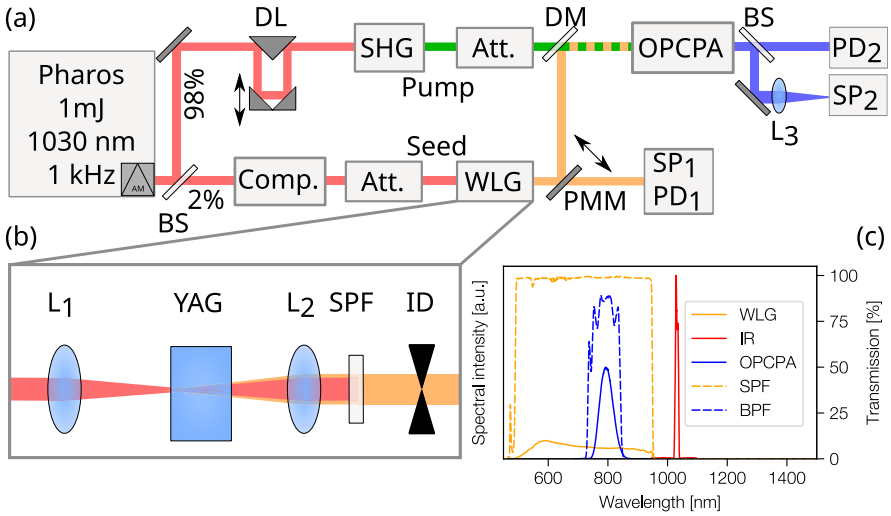

Fig. 1. Panel (a) shows the optical setup of the laser system with details of the WLG depicted in panel (b). Details and abbreviations are explained in the text. Panel (c) shows the spectrum of the drive laser (red), the WLG spectrum after the short pass filter (SPF, dashed line) in orange and the signal spectrum of the OPCPA stage (blue). Also shown is the spectral transmission of the band pass filter (BPF, dashed line) used to determine the seed energy in the WLG spectrum for the OCPA stage. Spectra have arbitrary scaling.

Pulses with approximately 20 uJ energy are tapped off from the main beam with a beam splitter and are sent to the seed section. The duration of the pulses is compressed from 500 fs (FWHM) to 170 fs (FWHM) in a transmission grating compressor (Comp.). The energy of the compressed pulses can be further controlled by an attenuator (Att.) consisting of a half-wave plate and a thin film polarizer. The beam out of the drive laser has a beam radius of 2.6 mm ($1/e^2$ intensity level) and a M^2 value of 1.1.

In the white light generation (Fig. 1(b)) sub 2 µJ pulses are focused with the lens L_1 (f = 100 mm) in the vicinity of the yttrium aluminum garnet (YAG) crystals input surface. The half angle divergence of the focused beam is around 20 mrad. The focusing lens L_1 is mounted on a linear stage to shift the focal spot along the beam propagation axis by 25 mm. With the geometrical focus located inside the crystal, abrupt broadening of the spectrum after the YAG could be observed for pulse energies >270 nJ, marking the onset of ultrafast white-light continuum generation [28]. Broadening of the output spectrum was accompanied with emerging plasma luminescence that could be observed from the side of the crystal. With input pulse energies above the filamentation threshold, the short wavelength side of the broadened spectrum extends to about 500 nm as depicted in Fig. 1(c). This is typical for WLG in YAG driven with pulses at 1030 nm central wavelength [20,29]. Furthermore, the cut-on wavelength changes only slightly with the focusing conditions.

An achromatic lens L_2 (f = 30 mm) after the YAG crystal is also mounted on a linear stage to collimate the beam. The collimation was adjusted using a wavefront sensor at a wavelength of 800 nm when the WLG drive pulse energy was changed. If the collimation was not adjusted after changing the WLG drive pulse energy, this is indicated in the text. The resulting beam radius is 1 mm at 800 nm. After the collimation spectral parts >950 nm are reflected by a short pass filter (SPF) to block the drive pulse and the red shifted part of the broadened spectrum. An iris (ID) is used to block the conical emission, i.e. the ring encircling the main intensity peak (Fig. 2(c)).

Optics EXPRESS

Subsequently, the filtered WLG beam is sent to a photodiode based energy head (PD_1) and a spectrometer (SP_2, OceanFX) or the OPCPA stage as a seed.

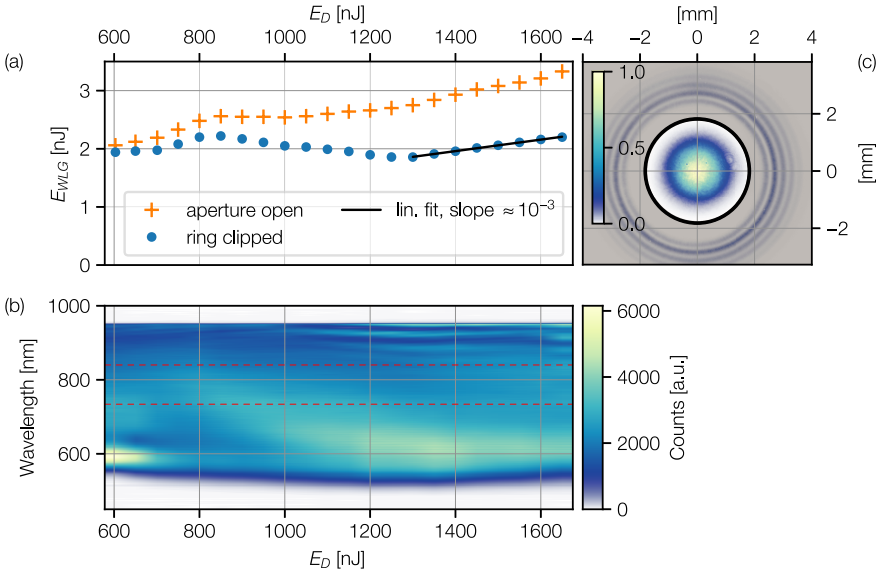

Fig. 2. Characteristics of the WLG stage output for the geometrical focus 0.2 mm in front of the YAG input surface. (a): Band-pass filtered pulse energy measured with PD_1. The energy contained in the main lobe is measured by clipping the conical emission with an iris diaphragm. (b): Evolution of the WLG spectrum driver pulse energy measured with SP_1. The FWHM transmission range for the BPF used in (a) is indicated by red dashed lines. (c): Beam profile after the collimation lens recorded with the same band pass filter used in (a). The edge of the iris diaphragm mentioned in (a) is indicated by a black line and the blocked area in grey.

2.2. OPCPA

The pump to seed pulse timing in the OPCPA stage can be adjusted with a motorized delay line (DL) located in the pump arm. 98 % of the initial pulse energy delivered by the drive laser is sent into a second harmonic generation (SHG) stage consisting of a 1 mm long β-barium borate (BBO) crystal. The frequency converted beam is split into two branches to pump two consecutive OPA stages. Here we only consider the first stage for our experiments. Pump and seed pulses are spatially overlapped on a dichroic mirror (DM) before they are sent into 3.5 mm long lithium triborate (LBO) crystal. The OPCPA is operated in a collinear geometry to avoid spatio-temporal couplings that can be caused by the more common non-collinear geometry [18,30] (see [27] for more details). To measure the OPCPAs pump energy while operating it a photodiode based energy head is placed in the back reflection of the pump beam on the LBO crystal. Due to the collinear setup of the OPCPA stage the fresh (front face) and depleted pump (back face) can not be separated spatially. For small modulation depths and the use of the signal as described in subsection 4.1, this had no detrimental effects. To avoid any influence of the signal or idler, the beam is filtered with a KG5 colored glass filter (T <10 % for wavelengths >780 nm).

After amplification in the OPCPA stage, the signal is reflected by two dielectric mirrors that transmit pump and idler wavelengths, separating the signal before it is collimated by an achromatic lens. A fraction of the signal pulse is split off with an uncoated fused silica beam sampler and focused onto the slit of a spectrometer (SP_2) with an achromatic lens (L_3). The

Optics EXPRESS

transmitted part of the signal is measured with a photodiode based energy head (PD_2). Both, the photodiode energy heads and the spectrometer after the OPCPA stage, are triggered with the same repetition rate as the PP, to measure single shots.

3. Spectral and spatial characteristics of the WLG

The output of WLG seeder for an OPCPA setup is usually optimized to deliver a flat, plateau like spectrum [17] or for maximum energy stability [20,23]. To achieve a stable output energy in the blue shifted part of the white light, the driver energy is chosen such that it is slightly below the threshold for a second pulse splitting event (refilamentation). The stability of the energy contained in the blue shifted part up to the driver wavelength can be better than the one the of driver pulses themselves, due to saturation effects [17].

In our case the blue shifted spectrum generated in the white light stage exceeds the phase matching bandwidth of the OPCPA stage (see Fig. 1(c)). Consequently, only a fraction of the broadened spectrum is amplified in the parametric process. Therefore, the energy in the spectral region overlapping with the phase matched wavelength range is of interest and not the whole energy in the WLG that is transmitted by the SPF. A band-pass filter (BPF) with 100 nm FWHM centered at 790 nm is used to filter the WLG spectrum to limit it to the phase matched wavelength range of the OPCPA stage.

Results shown in Fig. 2 are measured with a setup that was optimized with the geometrical focus set slightly before the YAG input surface. For this configuration the WLG drive energy was tuned between 600 nJ and 1650 nJ, measured before the YAG crystal. The onset of pulse splitting [31], i.e. rapid spectral broadening towards shorter wavelengths, was detected at 380 nJ. The threshold for refilamentation was measured at 1630 nJ.

The spectral range of the energy measurement depicted in Fig. 2(a) was limited with the BPF mentioned above. With the iris diaphragm open, so that the conical emission is included in the energy measurement, the seed energy for the OPCPA stage rises with the driver energy. It does not show signs of saturation close to the refilamentation threshold that is observed in other publications [20]. The reason for this could be that only a fraction of the blue broadened spectrum is considered for the energy measurement due to the BPF.

Figure 2(b) shows the evolution of the WLG spectrum up to 950 nm, limited by a SPF, with the FWHM of the BPF used for the pulse energy measurement in Fig. 2(a) indicated by red lines. Spectra were measured with a diffusor, a multi-mode fiber and a spectrometer that was not intensity calibrated. To establish a relation between the spectra they were scaled with the energy measured with the BPF. It can be seen from (b), that the blue broadened spectrum changes with the driver energy. Consequently also the energy contained in the spectral range that is transmitted by the BPF changes. Therefore the energy stability for a selection of the blue broadened spectrum (a) might be different than the whole blue broadened spectrum.

In our case it was observed that the signal spectrum after the OPCPA can show undesired ripples when the seed pulse contains the conical emission. Therefore, we blocked the conical emission after the WLG collimation lens with an iris diaphragm, which suppressed the ripples in the amplified spectrum. An image of the beam profile close to the collimation lens (L_2) is shown in Fig. 2(c). For the image the spectrum of the WLG beam is also limited with the BPF used in Fig. 2(a). The edge of the ID is depicted as a black line and the area obscured by the ID, which blocks the conical emission, is indicated in grey. The clear aperture diameter of the iris is 3.75 mm and the $1/e^2$ beam radius is 1.1 mm.

When the conical emission is blocked the filtered WLG pulse energy stays in a ± 10 % range around its average value (2.03 nJ) for a more than two fold increase of drive energy. Between 1300 nJ and 1600 nJ the slope for the filtered WLG energy is about 10^{-3}. Consequently the filtered WLG energy should be even more stable than the energy stability of the driver pulses, which is 0.15 % rms in this range. Even though the energy stability is expected to be better than 0.15 %

Optics EXPRESS

rms, it is no measure for the changes of the broadened spectrum that will subsequently influence the central wavelength after the OPCPA. Furthermore there are other effects like temporal chirp and focusing conditions of the seed pulse that don't affect the energy stability of the seed pulses. However, they can still affect the central wavelength after the OPCPA stage. Consequently a tool is needed that directly relates the effect of the WLG drive energy to the central wavelength after the OPCPA stage.

4. Reducing the central wavelength jitter of the amplified spectrum

Commonly, a WLG seed source is considered to be at its optimum working-point when the energy of the broadened output is most stable and the spectral region of interest is flat. Variations in WLG driver energy can lead to energy redistribution in the broadened spectrum (shown in Fig. 2(b)), resulting in changes of the amplified spectrum after the OPCPA and affecting the central wavelength. Furthermore, fluctuations of the drive energy will alter the position of the nonlinear focus within the bulk medium [32]. Prior to the nonlinear focus, the drive pulse propagates at the group velocity of its central wavelength, i.e. 1030 nm. The seed wavelengths for the subsequent OPCPA stage are generated with the onset of filamentation at the nonlinear focus. The seed pulse propagates at the group velocity of its central wavelength, which is 800 nm in this instance. The seed pulse arrival time at the OPCPA stage is influenced by the nonlinear focus position in the bulk material due to different group velocities between the driving pulse and the seed pulse within the remaining length of the YAG crystal [12]. Therefore λ_{COG} may shift in the amplified spectrum as a result of the relative timing change between seed and pump pulses in the OPCPA stage [12,18] due to drive energy changes.

Environmental fluctuations impact the optical path length of both the pump and seed pulse, thereby altering their arrival time at the OPCPA stage too. This, in turn, has a direct effect on the amplified output spectrum. In addition to temporal overlap, pointing jitter and drifts can further modify the spatial or temporal overlap, causing changes to the OPCPAs output spectrum.

As it is not possible to optimize individual parameters alone due to their strong couplings, we utilize a phase-sensitive detection scheme. This allows for a systematic analysis of the impact of a change in drive energy on λ_{COG} after the OPCPA stage. By isolating the impact of the drive laser output energy on the OPCPAs signal pulse spectrum, individual subsystems of the laser system, such as the WLG, can be optimized to minimize the influence of drive energy fluctuations.

4.1. Phase-sensitive amplitude measurement principle

In the following, the implementation of a phase-sensitive measurement [26] with sinusoidal modulation, named phase-sensitive amplitude measurement (PSAM), will be described. Firstly the pulse picker Pockels cell high voltage of the drive laser is modulated with a sinusoidal signal at 30 Hz. The modulation frequency was chosen to be higher than the typical $1/f$ noise in the setup. The modulation depth at 30 Hz in the drive lasers output energy was measured to be 0.14 % $\left(\Delta E_{IR}/\overline{E}_{IR}\right)$ while the mean output energy is at 94 % of its maximum. This modulation signal can then also be found in the pump pulse energy for the OPCPA and parameters of the amplified spectrum, e.g. the center of gravity wavelength (λ_{COG}) or the counts of one spectrometer pixel.

A schematic of the demodulation process for the central wavelength amplitude $\hat{\lambda}_{COG}$ is shown in Fig. 3. Perfect overlap of the data points for the OPCPAs pump pulse energy and the spectra, both measured for single shots, can be achieved by using the edges of the gated trigger signal (t_0 to t_1).

The modulation frequency f_{mod} is recovered from the OPCPAs pump pulse energy, by maximizing the demodulated amplitude ΔE in the frequency range ± 0.05 Hz around 30 Hz. The phase of the modulation signal ϕ is defined at the start of the data points at t_0, shown in Fig. 3(I). The pump energy signal level, which contains also the depleted pump, only changes slightly

Optics EXPRESS

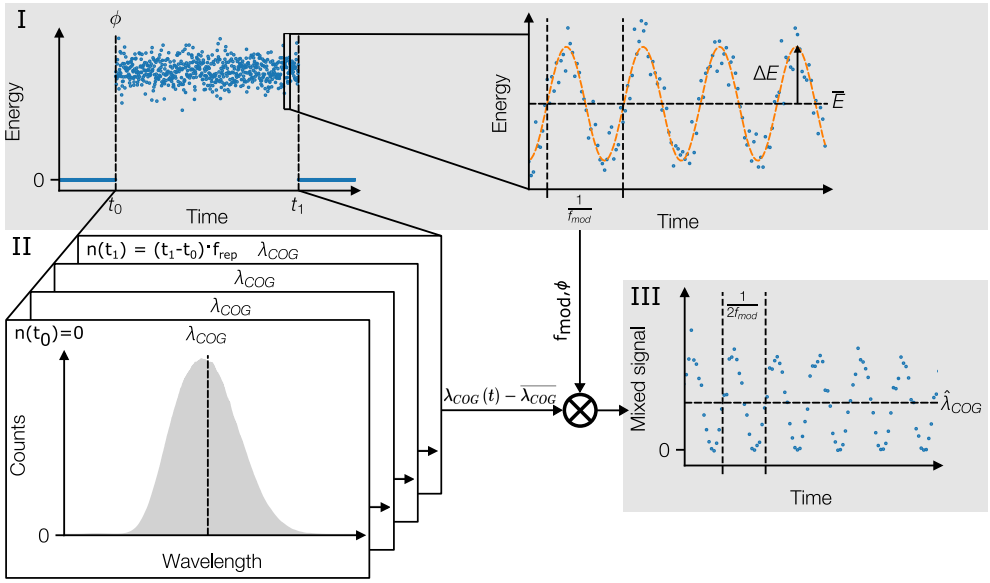

Fig. 3. Schematic of the evaluation for the phase-sensitive measurement. (I) the modulation frequency f_{mod} is found by maximizing the demodulation amplitude ΔE of the OPCPAs pump energy. The phase ϕ of the modulation signal is referenced at the start of the measurement t_0. (II) the central wavelength λ_{COG} of the OPCPA spectra recorded in parallel is calculated for every shot to derive the time series $\lambda_{COG}(t)$. (III) Mixed signal comprised of (I) and (II) containing the sum frequency and the difference frequency (DC part) which is proportional to the amplitude of the center of gravity wavelength $\hat{\lambda}_{COG}$.

with the energy transfer into the signal pulse. The average pump pulse energy is set to the same level for each experiment. Therefore the signal to noise ratio (SNR), defined as modulation amplitude ΔE over the standard deviation of the pulse energy (without modulation), is above 2 for all experiments. Other parameters like central wavelength, spectral width or integrated counts derived from the amplified spectrum can change drastically with the experimental setting for the WLG and do not provide a consistent SNR over the experiments.

From the recorded OPCPA signal pulse spectra the central wavelength λ_{COG} is calculated as the first moment after background subtraction in the following way:

$$\lambda_{COG} = \frac{\sum_{\lambda=\lambda_1}^{\lambda_2} \lambda I(\lambda)\, d\lambda}{\sum_{\lambda=\lambda_1}^{\lambda_2} I(\lambda)\, d\lambda}, \tag{1}$$

where λ_1 and λ_2 denote the edges of the region of interest in the spectrum. $I(\lambda)$ is the spectral intensity as counts and $d\lambda$ is the difference of the wavelengths on the edges for $I(\lambda)$.

From the time series of the central wavelength $\lambda_{COG}(t)$ its average $\overline{\lambda_{COG}}$ is subtracted and then mixed (multiplied) with a signal generated from the modulation frequency f_{mod} and its phase ϕ, which is shown in Fig. 3(II).

The mixed signal (III) contains the sum frequency and the difference frequency of all periodic signals in $\lambda_{COG}(t)$. When the frequency of the two signals that are mixed is the same, the difference frequency becomes zero, i.e. a DC offset. By averaging (low-pass filtering) the mixed signal, only the DC part remains. With only the modulation frequency contributing to the DC part, so other sources than the modulation are excluded. Hence, the influence of the driver lasers output energy on the central wavelength after the OPCPA can be precisely measured, even if it is small.

Optics EXPRESS

By choosing the correct amplitude for the modulation signal that is mixed with the time series of the central wavelength, the average of the mixed signal is equal to $\hat{\lambda}_{COG}$, which is its modulation amplitude. We assume that the influence of the modulated drive pulse energy is instantaneous, i.e. changes can be observed in the same pulse and there is no influence on the phase of the modulation signal. Hence, the calculated mean-to-peak amplitude of the center of gravity wavelength $\hat{\lambda}_{COG}$ can be in phase with the modulation signal or out of phase, which results in a negative amplitude.

Finally, we define the sensitivity of λ_{COG} to relative changes of the drive lasers output energy as:

$$S_\lambda = \frac{\hat{\lambda}_{COG} \cdot \overline{E}_{IR}}{\Delta E_{IR} \cdot 100\%} = \frac{\hat{\lambda}_{COG}}{0.14\%}. \tag{2}$$

Here, the relative amplitude of the drive lasers output energy is a constant of 0.14 % and the demodulated amplitude changes with the setup of the experiment.

In the following sections, PSAM is used as a post-processing tool to characterize and optimize the WLG and subsequent OPCPA stage.

4.2. Optimizing the position of the geometrical focus with PSAM

Changing the position of the geometrical focus of the driver laser with respect to the input surface of the YAG changes the energy range in which stable filamentation can be achieved. Furthermore it has an effect on the position of the nonlinear focus and the shape of the broadened spectrum, among others. To characterize the effects of a changed focus position on the WLG and the OPCPA stage, the position of lens L_1, shown in Fig. 1(b), was varied.

Figure 4(a) shows the driver pulse energy necessary to achieve pulse splitting over the position of geometrical focus, as the lower threshold for filamentation. The threshold for the first pulse splitting event is defined when the broadened spectrum reaches 633 nm on its blue side. When the geometrical focus is placed within the crystal the calculated peak power of the driving pulses at 170 fs duration corresponds well with the critical power of 1.37 MW found in literature [29]. This corresponds to a pulse energy of 270 nJ before reflection losses and is indicated by a black dashed line in Fig. 4(a). The refilamentation threshold was judged by the onset of strong modulation of the broadened WLG spectrum [12,16].

Geometrical focus positions between −0.76 mm and 1.37 mm correspond to the Rayleigh length for the focused driver beam around the input surface. Notably, in this range the threshold for refilamentation is increased, compared to positions well inside the YAG, i.e. >1.5 mm. The increased threshold for refilamentation could be related to the wave front curvature affecting the replenishing photon bath around the filament [33,34]. This leads to an expected increase of energy also in the broadened spectrum, only considering a constant conversion factor between driver pulse energy and WLG pulse energy.

Figure 4(b) shows results of PSAM, where the WLG driver energy E_D was set 10 % below the onset of refilamentation for each position of lens L_1. In addition the pulse energy in the amplification wavelength range of the OPCPA stage with the conical emission blocked (see Fig. 2) was measured. When the geometrical focus was located inside the YAG crystal, S_λ was measured to be around 0.15 $\frac{nm}{\%E_{IR}}$. Placing the geometrical focus more than 0.5 mm before the input surface resulted in S_λ >0.15 $\frac{nm}{\%E_{IR}}$. The lowest S_λ, i.e. the least sensitivity towards drive energy fluctuations, could be found with the geometrical focus placed approximately 200 µm before (A) and after the crystal (B), marked with vertical dashed lines in Fig. 4.

The blue part of the broadened spectrum generated with the settings described for set point A and B are shown in Fig. 5. Set point A delivers more than five times the energy (≈ 2 nJ after the filter) in the wavelength range that is phase matched in the OPCPA stage compared to set point B. This is probably caused by the increased drive energy for set point A but also the different shape of the broadened spectrum. Finally the lens position corresponding to A was chosen as the most

Optics EXPRESS

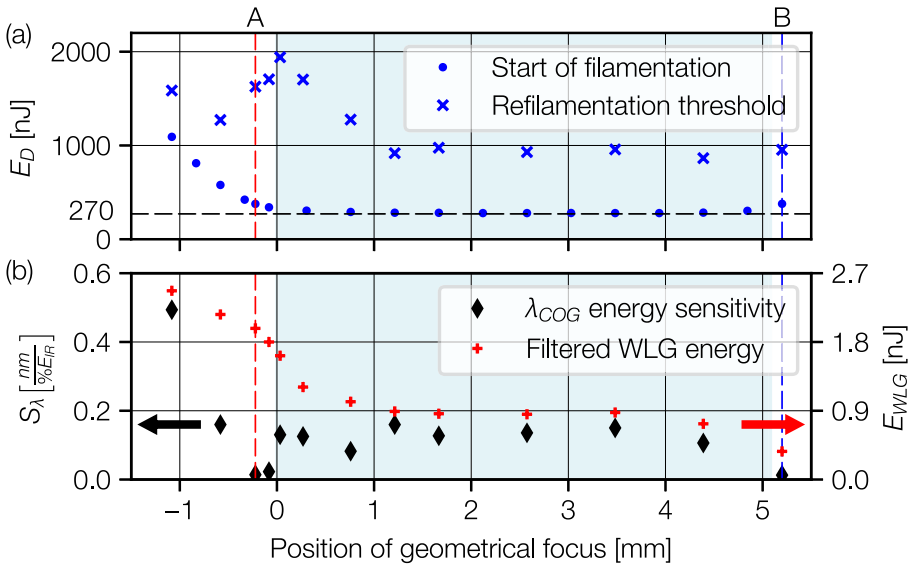

Fig. 4. (a): Pulse energy measured before the crystal input surface for the onset of filamentation and threshold for refilamentation over the geometrical focus position. YAG length indicated by blue shaded area. (b): Sensitivity of λ_{COG} after the OPCPA with respect to driver laser energy modulation over geometrical focus position. Filtered WLG energy in seeding range (see Fig. 2) over geometrical focus position.

promising for seeding an OPCPA stage as it provides the most energy in the seeding wavelength range and also a flat spectral intensity.

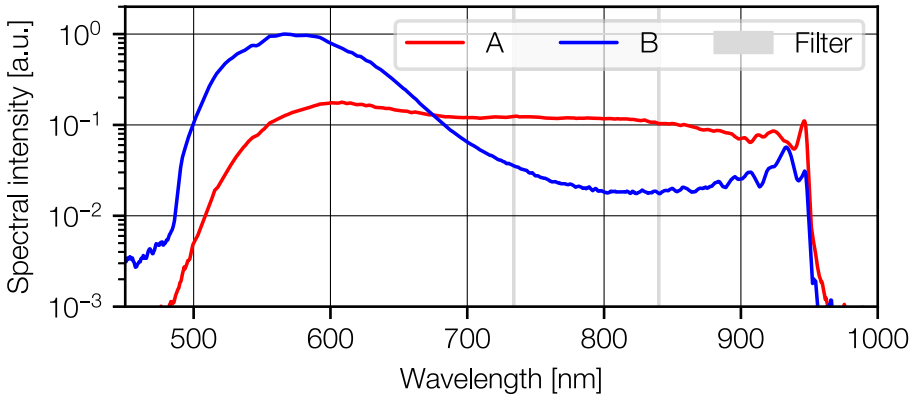

Fig. 5. Shown are the spectra measured for geometrical focus positions A and B, marked in Fig. 4. The grey area indicates the FWHM of the band pass filter used for seed energy measurements.

4.3. Effect of WLG driver energy on OPCPA wavelength stability

For further optimization of the OPCPA's performance the sensitivity of the central wavelength versus the drive laser pulse energy is now studied with PSAM at the found operation point. After the PSAM for each WLG drive energy, the OPCPA pump energy was varied step-wise

Optics EXPRESS

within −15 % to +7 % with the drive laser output unmodulated, to determine its influence on the OPCPAs central wavelength. The results are depicted in Fig. 6 and Fig. 7.

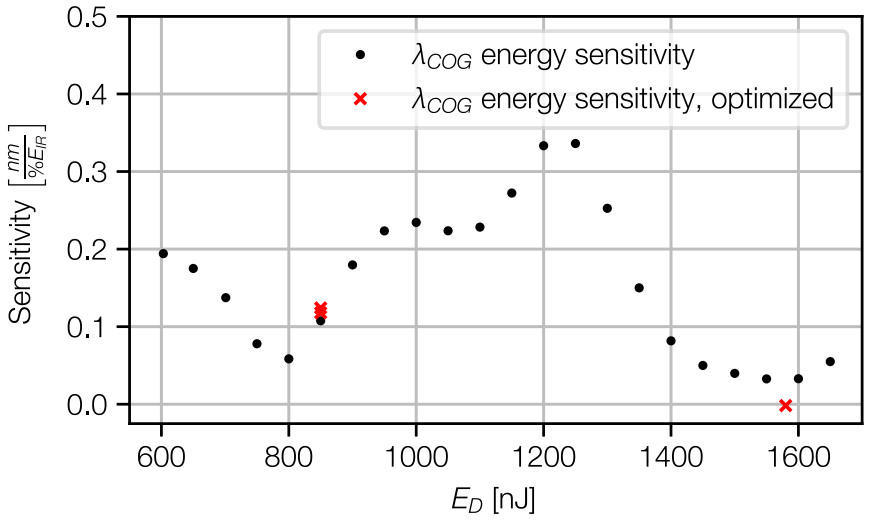

Fig. 6. Measured sensitivity (S_λ) of λ_{COG} on the WLG driver energy for set point A. For comparison, data points from other measurements are added in red.

As the position of the nonlinear focus is affected by the driver pulse energy [12,32], the DL was optimized to maximize the OPCPA output energy to account for the changed pump to seed pulse delay. This was only necessary for driver energies between 600 nJ and 1050 nJ, as the shift of the nonlinear focus position is negligible for drive energies >1050 nJ. The spatial alignment in the OPCPA stage and the position of the collimating lens L_2 were not changed during the measurements. To ensure that the WLG collimation lens position does not impact S_λ significantly, data points from other measurements, where the collimation lens position was optimized, were added for comparison.

The measured sensitivity shows no correlation to the seed energy, which is the same as shown in Fig. 2(a). This underlines the fact that the seed pulse energy stability is not the correct metric to optimize an OPCPA stage for minimum wavelength jitter.

The effects of the WLG driver pulse energy on the wavelength sensitivity can be further analyzed when the whole spectrum is considered instead of only the central wavelength. To accomplish this, the modulation amplitude and phase of each spectrometer pixels time series of counts are determined using PSAM. Again, modulation frequency and phase are obtained from the measured pump pulse energy to then demodulate the amplitude of counts ($\Delta I_{Mod}(\lambda)$) at every spectrometer pixel (wavelength). This demodulated signal contains the influences of the WLG ($\Delta I_{WLG}(\lambda)$) and the pump energy ($\Delta I_{Pump}(\lambda)$).

The central wavelength's dependence on the OPCPA pump energy can be determined by analyzing the measurements obtained by varying the pump energy attenuator. Every spectrometer pixel count $I(\lambda)$ over the pump energy E_{Pump} is fitted with a second order polynomial. The linear slope $\left(\frac{dI_{Pump}(\lambda)}{dE_{Pump}}\right)$ is calculated at the working point of 13 µJ and multiplied with the measured pump energy modulation amplitude $\hat{E}_{Pump}$. By subtracting the isolated influence of the pump pulse energy from the demodulated signal of the sensitivity measurement, it is possible to quantify the effect of the WLG on the amplified spectrum ($\Delta I_{WLG}(\lambda)$):

$$\Delta I_{WLG}(\lambda) = \Delta I_{Mod}(\lambda) - \Delta I_{Pump}(\lambda) = \Delta I_{Mod}(\lambda) - \hat{E}_{Pump} \times \frac{dI_{Pump}(\lambda)}{dE_{Pump}}. \tag{3}$$

Optics EXPRESS

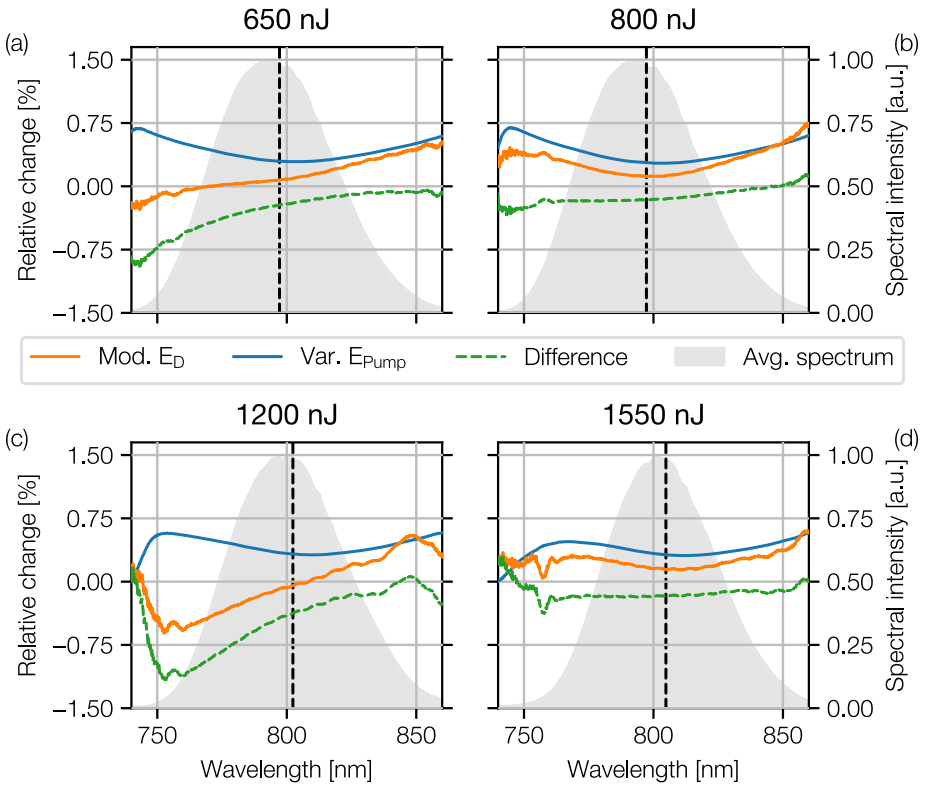

Fig. 7. Shown is the average spectrum during the energy modulation measurement in grey. The relative change of the spectrum in the positive peak of the modulation for selected WLG driver energies is depicted in orange (Mod. E_D). Depicted in blue is the relative change of the average spectrum calculated from variation of the OPCPAs pump energy and the positive modulation amplitude of the pump energy (Var. E_{Pump}). The influence of the WLG alone is the difference between the former and depicted in a dashed green line (Difference). Details on the calculation are in the text.

Figure 7 shows the results when this method is applied to a selection of WLG driver pulse energies E_D of 650 nJ (a), 800 nJ (b), 1200 nJ (c) and 1550 nJ (d). The demodulated amplitudes are depicted relative to the average spectrum $\overline{I(\lambda)}$. The driver pulse energies are the same as in Fig. 6 and correspond to sensitivities of 0.18 $\frac{nm}{\%E_{IR}}$(a), 0.06 $\frac{nm}{\%E_{IR}}$(b), 0.33 $\frac{nm}{\%E_{IR}}$ (c) and 0.03 $\frac{nm}{\%E_{IR}}$(d). The central wavelength of the mean spectrum is indicated by the black dashed line.

In Fig. 7(a) and (c) the phase sensitivity part of PSAM can be observed. A rising pump energy causes rising spectral intensity in some part of the OPCPAs spectrum, i.e. being in phase with the pump energy, while others show falling spectral intensity and are out of phase. The effect reverses when the pump energy is reduced, i.e. when the amplitude is negative in the second half of the modulation period. The described mechanism causes spectral intensity in the spectrum to be transferred between the red and blue edge of the OPCPAs spectrum for every half cycle of the modulation. For Fig. 7(c), where S_λ is at its maximum, this results in a relative count loss of -3.6×10^{-6}. This means that spectral intensity is mainly shifted between spectrometer pixels, while there is an effective loss for an increased pump energy.

In comparison for (b) and (d) the spectral intensity is in phase with the pump energy modulation, i.e. increase for all wavelength for a rising pump energy and reduces for decreasing pump energy. For (d), where S_λ is at its minimum, this results in a relative count gain of the spectrum of

Optics EXPRESS

2.1×10^{-3}. However, with every spectrometer pixel gaining equally between 0.5 % and 0.75 % evenly distributed over the spectrum, the effect on λ_{COG} is small.

With the measurements described above the influence of the driver lasers energy can now be separated between OPCPA pump energy and WLG. For all cases shown in Fig. 7 the influence of the OPCPAs pump energy on the amplified spectrum, shown in blue, is negligibly small $\left(<5\frac{pm}{\%E_{IR}}\right)$ due to saturation effects. It can therefore be concluded that the sensitivity of the central wavelength with respect to the driving laser pulse energy is mainly determined by the WLG.

For the range between 950 nJ and 1350 nJ shown in Fig. 6 the increased sensitivity with respect to energy modulation can be attributed to the shift of spectral intensity between the blue and red edge of the spectrum depicted in Fig. 7(d). Which effect in the WLG causes the differences between (a)+(c) and (b)+(d) is unclear. A possible reason could be the change of spectral intensity with WLG drive energy in the seeding spectrum, like depicted in Fig. 2(b). However, with PSAM the passive wavelength stability with respect to driver laser energy fluctuations could be optimized. A reduction of ≈ 40 % of uncorrelated contributions to the central wavelength jitter can be calculated between the highest sensitivity at 1250 nJ and the lowest sensitivity at 1550 nJ (Fig. 6). The influence of pump to seed pulse timing [12] is described in the next section.

4.4. *Influence of seed to pump timing*

With parametric amplification being an instantaneous process [10] the pump to seed pulse time delay can affect the central wavelength of the amplified spectrum. For example the pump intensity for each wavelength in the positively chirped seed pulse (≈ 200 fs) is changed due to the temporal envelope of the pump pulse (≈ 500 fs). To evaluate the influence of pump to seed pulse delay in our OPCPA setup, dedicated scans were carried out with the delay stage (see Fig. 1). The effect of the delay on the amplified spectrum is measured in the change of counts on the spectrometer. The normalized difference in counts to the averaged spectra at 0 fs delay is depicted in Fig. 8(a). The timing delay was scanned twice in eight steps over the range of ≈ ± 13 fs. For each delay position approximately 2000 spectra were recorded. For the analysis 125 spectra at the beginning and end of each position are discarded to exclude effects of a still moving stage. This results in >7000 spectra recorded for delay position between −10 fs and +10 fs. At the reverse points, i.e. at ± 13.3 fs, >3500 spectra were recorded. The recorded spectra are averaged for each delay step. A reference spectrum is calculated at delay 0 fs as the average over all spectra recorded at this delay. Subsequently the reference spectrum is subtracted form the spectra recorded at other delay steps, to calculate the difference in counts on the spectrometer. Finally this data is normalized by the absolute maximum deviation from the reference spectrum.

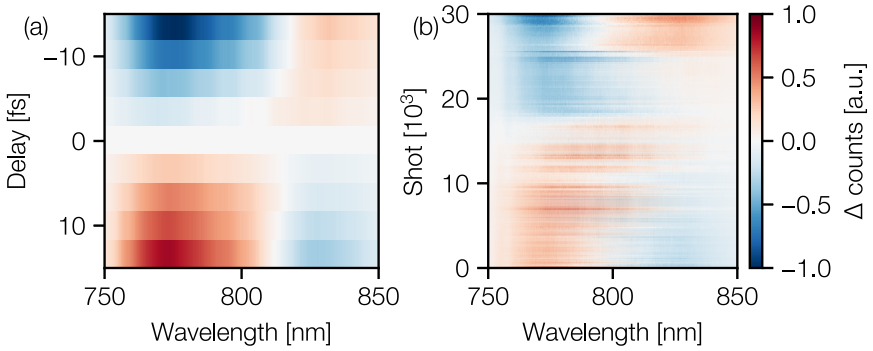

Fig. 8. Difference to the mean spectrum normalized to the maximum deviation. (a) for delay steps. Mean spectrum is at delay 0 fs. (b) free running and filtered with a 5 Hz low pass filter and sorted for central wavelength.

Optics EXPRESS

As can be seen from Fig. 8(a), for positive delays, i.e. later pump pulses, the red edge of the spectrum has less counts and the blue edge of the spectrum has more counts. In conclusion, the central wavelength and spectral intensity shifts to shorter wavelength with positive delay and vice versa for negative delays. The shift of λ_{COG} with respect to the pump to seed pulse delay was measured to be between −65 pm/fs (0.12 %/fs, relative central wavelength shift over FWHM bandwidth) for 650 nJ WLG drive energy and −48 pm/fs (0.10 %/fs, relative central wavelength shift over FWHM bandwidth) for 1550 nJ of WLG drive energy. These values are similar to what was measured in other setups [18] (46 pm/fs).

The OPCPA system used for the experiments showed a slow variation of the central wavelength around its set point with a time scale of several seconds. To analyze these variations, the spectra recorded over 30 s were filtered with a 5 Hz low-pass filter and sorted in ascending order for their central wavelength. Subsequently the average over all spectra was subtracted and the remaining counts were normalized to the absolute deviation, like for the delay scan. The results are shown in Fig. 8(b).

At zero shots, the maximum negative deviation in central wavelength results in a spectrum with more spectral intensity in the blue edge and less spectral intensity in the red edge compared to the averaged spectra. The opposite is true for the maximum wavelength at the highest shot number. The spectral change appears similar to that observed in Fig. 8(a) for a temporal delay between the pump and seed pulses. It can be concluded that drifts between pump and seed pulse timing contribute to slow changes in the central wavelength. However, the characteristic shift of energy in the amplified spectrum after the OPCPA stage cannot be observed for a modulation of the driver laser energy if the WLG stage has been optimised for best wavelength stability of the OPCPA (Fig. 7(d)). Therefore, it can be assumed, that the driver energy variation does not cause a significant time delay between pump and seed pulses at the optimized point of operation. In order to further improve the wavelength stability, the pump to seed delay needs to be actively stabilized.

4.5. Active stabilization of timing drifts

To stabilize the timing delay between the pump and seed pulses, an actuator is placed in the collimated WLG arm before the OPCPA stage. In our case, a 4 mm diameter mirror was mounted on a piezo stack as a folding mirror (PMM). The stroke of 13 μm resulted in an achievable delay range of about ± 45 fs, which is enough to compensate the drifts of <20 fs that were observed over several tens of hours. The typical sensitivity of λ_{COG} when the seed pulse is delayed relative to the pump pulse was 100 pm/fs at this specific operation point of the OPCPA stage. Spectrometer SP_2 was used to measure the spectra from which λ_{COG} was calculated for the error signal. A digital PI-loop was used to directly stabilize the central wavelength with the PMM as actuator. The cycle time of the PI-loop was ≈ 240 Hz. An additional spectrometer was used in place of PD_2 to measure the spectra out of loop.

Open loop (OL) performance is shown for times <0 s and closed loop (CL) performance for times >0 s in Fig. 9(a). The integrated jitter for OL and CL operation shown in 9(b) is calculated from 30 s long sections. In Fig. 9(b) it can be seen that two thirds of the integrated jitter in OL operation are located at frequencies <10 Hz, i.e. slow drift. In CL operation λ_{COG} drifts up to 6 Hz can be compensated. Above 10 Hz white noise contributions to the central wavelength on the in-loop spectrometer (SP_2) dominate, which cannot be compensated. The upper limit of the timing jitter in closed loop operation can then be calculated to <0.3 fs. The integrated wavelength jitter over one minute is then 28.6 pm or 0.06 % of the spectral FWHM.

Optics EXPRESS

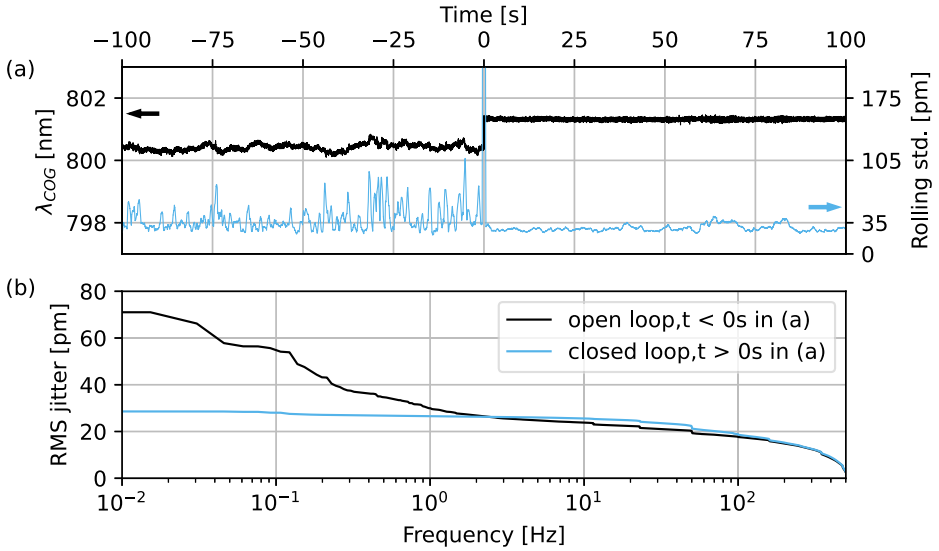

Fig. 9. (a): λ_{COG} and its rolling standard deviation for 1000 values over time in open loop (t < 0) and closed loop operation (t > 0). The spectra for evaluation of λ_{COG} were recorded out of loop. (b): Integrated jitter for open loop and closed loop operation from (a). The PI controller mainly suppresses drifts up to 6 Hz.

5. Conclusion

This paper presents the optimization of bulk white light generation for central wavelength stability in the subsequent OPCPA stage, which is seeded by the WLG. We have demonstrated that optimizing the output of a WLG seeder for the best pulse energy stability of the broadened spectrum does not result in the best performance of the subsequent OPCPA stage.

We have implemented a technique called PSAM to isolate influences on the central wavelength of the amplified spectrum. This includes pulse energy fluctuations of the drive laser. By using the PSAM method, we were able to enhance the passive stability of the OPCPA by minimizing the influence of the drive laser's pulse energy on the OPCPA's central wavelength. For an optimized setup, the center of gravity shift of a spectrum supporting sub-25 fs pulses at 800 nm can be less than 10 pm per percent of driver pulse energy variation.

Detailed investigations of driver laser energy on the OPCPA's output spectrum have shown that the WLG output characteristics have a larger impact on the central wavelength compared to the OPCPA's pump pulse energy. Comparing results of PSAM on an optimized operation point to measurements of the pump to seed pulse delay it can be concluded that the WLG drive pulse energy has a negligible effect on the seed pulse delay. Still, it was found that environmental changes influence the pump to seed pulse delay in the OPCPA stage, deteriorating the central wavelength stability performance.

To compensate for environmental effects a digital PI-loop acting on the optical path length in the WLG arm of our OPCPA system was implemented. By stabilizing the pump to seed delay to be below 0.3 fs a wavelength jitter of <30 pm, measured out of loop, was achieved.

Ultimately, optimizing our WLG seeder with PSAM and mitigating environmental influences by active stabilization of the pump pulse to seed pulse delay allowed us to reach a relative wavelength stability of $<4 \times 10^{-5}$ which exceeds the requirements for LWFA [6] and FEL seeding [5].

Optics EXPRESS

We believe that PSAM is an excellent tool to characterize and optimize complex systems that show intricate couplings between input and output parameters. This is not limited to WLG seeded OPCPA systems but could also be used in other nonlinear optics systems with similar complexities.

Funding. Deutsche Forschungsgemeinschaft (491245950).

Acknowledgements. The authors thank Dr. Skirmantas Ališauskas (DESY, Hamburg) and Dr. Aradhana Choudhuri (formerly DESY, Hamburg) for valuable discussions and Dr. Samuell Hartwell (DESY, Hamburg) for proofreading. We appreciate support from the workshops and technical groups of DESY.

Disclosures. The authors declare no conflicts of interest.

Data availability. Data underlying the results presented in this paper are not publicly available at this time but maybe obtained from the authors upon reasonable request.

References

1. T. Tajima and J. M. Dawson, "Laser electron accelerator," Phys. Rev. Lett. **43**(4), 267–270 (1979).
2. E. Esarey, C. B. Schroeder, and W. P. Leemans, "Physics of laser-driven plasma-based electron accelerators," Rev. Mod. Phys. **81**(3), 1229–1285 (2009).
3. E. Allaria, R. Appio, L. Badano, *et al.*, "Highly coherent and stable pulses from the FERMI seeded free-electron laser in the extreme ultraviolet," Nat. Photonics **6**(10), 699–704 (2012).
4. A. R. Maier, N. M. Delbos, T. Eichner, *et al.*, "Decoding sources of energy variability in a laser-plasma accelerator," Phys. Rev. X **10**(3), 031039 (2020).
5. T. Lang, M. M. Kazemi, J. Zheng, *et al.*, "High repetition rate, low noise and wavelength stable OPCPA laser system with highly efficient broadly tunable UV conversion for FEL seeding," EPJ Web Conf. **267**, 01052 (2022).
6. M. Kirchen, S. Jalas, P. Messner, *et al.*, "Optimal beam loading in a laser-plasma accelerator," Phys. Rev. Lett. **126**(17), 174801 (2021).
7. A. Jullien, O. Albert, F. Burgy, *et al.*, "10^{-10} temporal contrast for femtosecond ultraintense lasers by cross-polarized wave generation," Opt. Lett. **30**(8), 920–922 (2005).
8. T. J. Yu, S. K. Lee, J. H. Sung, *et al.*, "Generation of high-contrast, 30 fs, 1.5 PW laser pulses from chirped-pulse amplification ti:sapphire laser," Opt. Express **20**(10), 10807–10815 (2012).
9. C. Manzoni and G. Cerullo, "Design criteria for ultrafast optical parametric amplifiers," J. Opt. **18**(10), 103501 (2016).
10. S. Witte and K. S. E. Eikema, "Ultrafast optical parametric chirped-pulse amplification," IEEE J. Sel. Top. Quantum Electron. **18**(1), 296–307 (2012).
11. C. Teisset, N. Ishii, T. Fuji, *et al.*, "Optical synchronization for OPCPA chains," Ultrafast Opt. V **132**, 535–545 (2007).
12. R. Riedel, M. Schulz, M. J. Prandolini, *et al.*, "Long-term stabilization of high power optical parametric chirped-pulse amplifiers," Opt. Express **21**(23), 28987–28999 (2013).
13. S. Prinz, M. Häfner, M. Schultze, *et al.*, "Active pump-seed-pulse synchronization for OPCPA with sub-2-fs residual timing jitter," Opt. Express **22**(25), 31050–31056 (2014).
14. R. R. Alfano and S. L. Shapiro, "Observation of self-phase modulation and small-scale filaments in crystals and glasses," Phys. Rev. Lett. **24**(11), 592–594 (1970).
15. A. Couairon and A. Mysyrowicz, "Femtosecond filamentation in transparent media," Phys. Rep. **441**(2-4), 47–189 (2007).
16. A. Dubietis and A. Couairon, *Ultrafast supercontinuum generation in transparent solid-state media* (Springer, 2019).
17. M. Bradler, P. Baum, and E. Riedle, "Femtosecond continuum generation in bulk laser host materials with sub-μJ pump pulses," Appl. Phys. B: Lasers Opt. **97**(3), 561–574 (2009).
18. K. Mecseki, M. K. R. Windeler, A. Miahnahri, *et al.*, "High average power 88 W OPCPA system for high-repetition-rate experiments at the LCLS x-ray free-electron laser," Opt. Lett. **44**(5), 1257–1260 (2019).
19. I. Tamer, M. Hellwing, Y. Azamoum, *et al.*, "Few-cycle fs-pumped NOPA with passive ultrabroadband spectral shaping," Opt. Express **28**(13), 19034–19043 (2020).
20. L. Indra, F. Batysta, P. Hříbek, *et al.*, "Picosecond pulse generated supercontinuum as a stable seed for OPCPA," Opt. Lett. **42**(4), 843–846 (2017).
21. N. Ishii, M. Maruyama, K. Nagashima, *et al.*, "Generation and compression of an intense infrared white light continuum in YAG irradiated by picosecond pulses," Opt. Express **29**(11), 17069–17076 (2021).
22. T. Metzger, C. Grebing, C. Herkommer, *et al.*, "High-power ultrafast industrial thin-disk lasers," in *2019 IEEE Photonics Conference (IPC)*, (IEEE, 2019), pp. 1–2.
23. L. Roškot, O. Novák, B. Csanaková, *et al.*, "Importance of crystal length on the stability of a picosecond supercontinuum generated in undoped YAG," J. Opt. Soc. Am. B **40**(6), 1391–1397 (2023).
24. D. Majus and A. Dubietis, "Statistical properties of ultrafast supercontinuum generated by femtosecond Gaussian and Bessel beams: a comparative study," J. Opt. Soc. Am. B **30**(4), 994–999 (2013).

Optics EXPRESS

25. V. Jukna, N. Garejev, G. Tamošauskas, *et al.*, "Role of external focusing geometry in supercontinuum generation in bulk solid-state media," J. Opt. Soc. Am. B **36**(2), A54–A60 (2019).
26. D. Blair and P. Sydenham, "Phase sensitive detection as a means to recover signals buried in noise," J. Phys. E: Sci. Instrum. **8**(8), 621–627 (1975).
27. T. Eichner, T. Hülsenbusch, J. Dirkwinkel, *et al.*, "Spatio-spectral couplings in saturated collinear OPCPA," Opt. Express **30**(3), 3404–3415 (2022).
28. A. Brodeur and S. Chin, "Ultrafast white-light continuum generation and self-focusing in transparent condensed media," J. Opt. Soc. Am. B **16**(4), 637–650 (1999).
29. A.-L. Calendron, H. Çankaya, G. Cirmi, *et al.*, "White-light generation with sub-ps pulses," Opt. Express **23**(11), 13866–13879 (2015).
30. M. Pergament, M. Kellert, K. Kruse, *et al.*, "High power burst-mode optical parametric amplifier with arbitrary pulse selection," Opt. Express **22**(18), 22202–22210 (2014).
31. A. L. Gaeta, "Catastrophic collapse of ultrashort pulses," Phys. Rev. Lett. **84**(16), 3582–3585 (2000).
32. J. Marburger, "Self-focusing: Theory," Prog. Quantum Electron. **4**, 35–110 (1975).
33. A. Jarnac, G. Tamosauskas, D. Majus, *et al.*, "Whole life cycle of femtosecond ultraviolet filaments in water," Phys. Rev. A **89**(3), 033809 (2014).
34. L. Bergé, S. Skupin, R. Nuter, *et al.*, "Ultrashort filaments of light in weakly ionized, optically transparent media," Rep. Prog. Phys. **70**(10), 1633–1713 (2007).